CrossMark

Principle and Application of Tip-enhanced Raman Scattering

Changzhong Gao[1] · Weihua Lin[2] · Jiangcai Wang[2] · Rongming Wang[2] · Jingang Wang[3]

Abstract Tip-enhanced Raman scattering (TERS), as a combination of scanning probe microscopy (SPM) and surface-enhanced Raman spectroscopy (SERS) makes a huge progress in high sensitive optical and spectral analysis field by plasmon and plasmonic gradient enhancement. We introduce the mechanisms and setup of TERS with several experimental cases. Among them, high-vacuum tip-enhanced Raman spectroscopy (HV-TERS) is introduced in detail by describing the plasmon-driven reactions.

Keywords Plasmon · Tip-enhanced Raman spectroscopy

Introduction

Raman signals can provide substantial chemical information about the target molecules, so the desire for enhanced Raman signals necessitates a new approach. When the target molecule adsorbed onto the metal surface, the signals can be enormously enhanced because of surface plasmon resonance (SPR).

Changzhong Gao and Weihua Lin contributed equally.

✉ Rongming Wang
  rmwang@ustb.edu.cn

✉ Jingang Wang
  jingang_wang@sau.edu.cn

1 School of Physics, Beihang University, Beijing 100083, People's Republic of China

2 Beijing Key Laboratory for Magneto-Photoelectrical Composite and Interface Science, School of Mathematics and Physics, University of Science and Technology Beijing, Beijing 100083, People's Republic of China

3 Department of Physics, Liaoning University, Shenyang 116023, People's Republic of China

Surface plasmon (SPs) is the free electron's collective oscillations excited by the incident laser on the interface between metal and dielectric media. And, the surface plasmon resonance (SPR), excited by an excitation laser, can enormously enhance the localized electromagnetic field with the help of a sharp metal tip and the metal film substrate. Besides, the spatial resolution can be significantly increased. In the meantime, the enhanced electromagnetic field is considered as the physical enhancement mechanism for SERS [1–3] and TERS [4–8].

Therefore, as a combination of SPM and SERS, TERS makes a huge progress in high sensitive optical and spectral analysis field by plasmon and plasmonic gradient enhancement.

SERS can contribute to the electric field enhancement which is approximately 10^8–10^{11} and chemical enhancement which is only 10^2–10^3. Because of LSPR [9–11] which can enhance the Raman spectrum over a large frequency range, the sensitivity of Raman spectroscopy can be enormously enhanced, and the Raman imaging can be observed simultaneously to provide a more explicit evidence for spectral analysis [12, 13]. Besides, changes in the electronic structure of adsorbed molecules can lead to the chemical enhancement, and therefore, some Raman peaks can be enhanced selectively and obviously.

As the key technique of TERS, SERS, which can overcome the limitation of low Raman scattering cross section by optical diffraction, is used for detecting the chemical information and vibration modes of molecules. Moreover, SERS signals show the averaged information of randomly adsorbed molecules. Instead of measuring the certain molecule, SERS experiments can only be performed statistically. So, it is hard to achieve single molecule resolution in experiment [14–16].

To overcome the shortcomings of spatial resolution and limitation of substrates in SERS, the idea of TERS came up

🗍 Springer

as the combination of SERS and SPM technologies in 1985 by Wessel [5]. Then, Zenobi, Kawata, Anderson, and Pettinger first reported TERS results in 2000 [4, 6–8], independently. Since then, the feasibility of TERS is demonstrated widely around the world [17–19]. There are several groups [20–23] who can achieve single-molecule detection and mapping at the resolution level of a single molecule. But, in the first beginning, the technique is insufficient to distinguish the specific parts of a molecule with a molecular resolved level. In this way, many researchers were focused on revealing the mechanism of TERS, and then, TERS was developed into a nanoimaging method and can make a big progress in studying surface science. There are several excellent review papers about that [20–27].

Mechanisms

TERS plays an important role in surface science, even at submolecular level [28, 29]. The spatial resolution is enormous enhanced by using a sharp metal tip. And by using the SPM controller, the gap distance between the substrate and the tip can be controlled effectively.

As mentioned above, surface plasmon resonance (SPR) can be used to obtain the localized electromagnetic enhancement and hence to create "hot site." And, because of the existence of hot site, the Raman scattering for TERS can be enormously enhanced. The energy of light is concentrated in a very tiny area, where the interaction between the light and matter can be significantly enhanced. And, the spatial resolution of TERS signals is about 1~10 nm.

In the first beginning, the highest resolution is approximately 200 nm in the range of visible light because of the optical diffraction according to the Abbe formula:

$$\Delta x = 0.61\lambda \Big/ \mathrm{NA}$$

which is too low for nanoscience. Besides, the conventional Raman microscopy is not capable to obtain the chemical information of the nanocomposition and distribution of the specimen. Therefore, thousands of researchers have attempted to improve the spatial resolution. With the development of microscopy, the resolution, which is depending on the wavelength of incident light and numerical aperture (NA) of the object, has been developed rapidly. In 2000, the TERS were reported by four groups with a reduced spatial resolution (approximately 50 nm) [4, 6–8].

Besides, another important concept is the enhancement factor of TERS. In considering the enhancement that is mostly originated from the electric field enhancement in TERS, the factor can be written as

$$g = E_{\mathrm{Tip}} \Big/ E_0$$

where E_{Tip} and E_0 are the intensities of the enhanced electric field under the metal or metal-coated tip and the incident electric field.

Types of TERS

Among the varied SPM technologies, scanning tunnel microscope (STM), atomic force microscopy (AFM), shear force microscopy (SFM), and scanning near-field optical microscopy (SNOM) systems are usually used in the TERS setup.

As shown in Fig. 1a, by controlling the distance between the tip (metal or metal-coated) and substrate (approximately a few nanometers) by SPM, the enormous electric field coupling between the tip and substrate is induced. Because of the created hot spot, the enhancement area is strongly limited underneath the tip apex.

The STM system can image surface at atomic resolution (0.1 nm). When distance between the conducting tip and surface of the target is close enough, electrons can tunnel through the barrier between the tip and the surface with the help of a bias voltage, as shown in Fig. 1b. In this way, the tunneling current is very sensitive to the distance of the tip and surface. The high control precision of STM provides a powerful method to study single molecules. However, a conductive substrate or a conductive substrate covered with ultra-thin sample is required in STM. Besides, STM needs to be performed in an ultra-high-vacuum (UHV) and low-vibration-noise environment. And, a low-temperature (LT) environment is required to reduce thermal drifts [23]. The advantages of STM-TERS are that it has high control precision and high spatial resolution, but it is difficult to build and is not suitable for many samples, such as bio-specimen.

Moreover, AFM and SFM system are basically based on the tip interaction with the topography of the sample and subsequent change in deflection (contact mode) and amplitude/phase (tapping mode) [27]. The way AFM works is utilizing the atom force between the tip and the substrate as shown in Fig. 1c. Besides, in AFM testing, it does not require specific samples or treatments that make it a universal and effective method. Any surface can be applied, even the rough one with a few microns thick. Specially, AFM can be used in a liquid environment. In this way, AFM-TERS got a great advantage in biological [31–35] and organic researches. Moreover, it also presents many shortcomings, such as the Au/Ag-coated tips which are needed to create the hot spot and easily break during AFM scanning.

Therefore, the SFM is usually used in the TERS setup. As shown in Fig. 1d, a metal tip can be used to detect surface shear force because of the lateral interaction between the sample and the tip [36]. The amplitude and phase of the tuning fork which is connecting with the metal tip can be surveyed by using high-speed electronics. Contrasting with AFM-TERS, SFM-SERS can also be
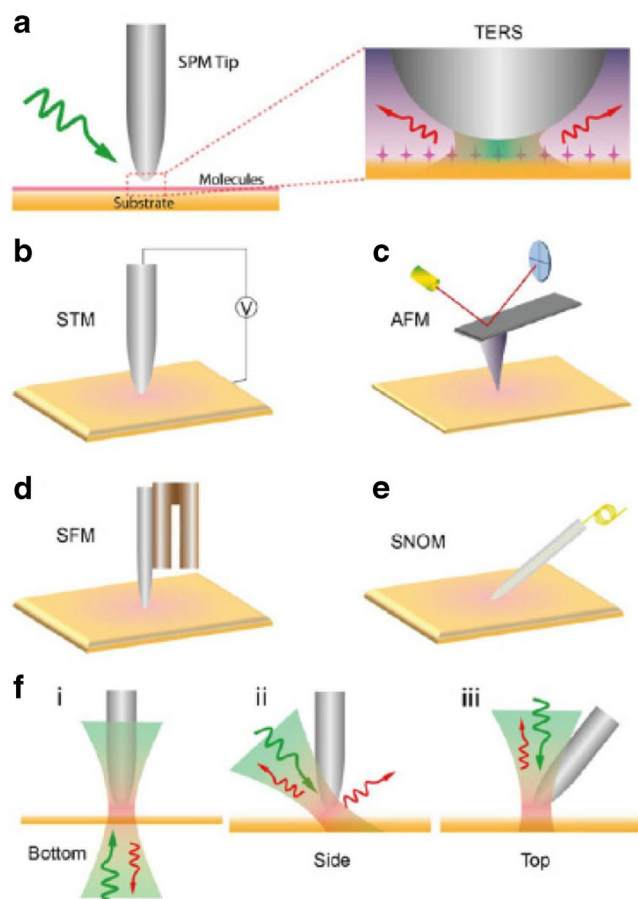
Fig. 1 **a** Schematic illustration of TERS. **b–e** Schematic illustration of STM, AFM, SFM, and SNOM. **f** Three different modes of excitation and collection: side excitation and side collection (*i*), bottom excitation and bottom collection (*ii*), and top excitation and top collection (*iii*). Adapted from Ref [30]

used in liquid environment and for any samples [37]. Besides, the metal tips used in SFM-TERS are more stable than the Au/Ag-coated tips in AFM-SERS [38, 39]. In the other side, SFM has a poor lateral resolution because of the oscillation amplitudes of the tuning fork [39, 40].

Moreover, by exploiting the evanescent waves on the surface of samples, as shown in Fig. 1e, SNOM can achieve high resolution and artifact images with the help of two types of feedback, including shear force (same as SFM) and constant force (same as AFM). Specially, the resolution of SNOM is approximately 20 nm which is restricted by the size of the detector aperture instead of the excitation laser. Apparently, a sharp tip is needed to obtain a higher resolution.

Setup

The enhancement of TERS includes the chemical enhancement and electric field enhancement. Noble metals [27], such as Au/Ag/Cu, are used as the tips and substrates usually, due

to their good optical response and large electric field enhancement in the visible light region.

Tip and Substrates

In TERS, a metal or metal-coated sharp tip apex (approximately 10~50 nm) can contribute to a highly localized surface charge density. It plays an important role in influencing the enhancement factor of TERS. Besides, the spatial resolution of TERS is increased, as well as the imaging quality of the SPM [41–45].

In some specific systems, such as AFM-TERS, a metal-coated Si or Si_3N_4 tip is used frequently. Normally, the silver or gold would be evaporated onto the probe surface in a high-vacuum (HV) system. The diameter of the metal-coated tip apex is approximately 20–50 nm, while the thickness of the coated metal film is several tens of nanometers, as shown in Fig. 2a [45, 46]. The oxidation of the silver tips leads to a decrease in the enhancement factor [50].

In STM- and SFM-TERS systems, an electrochemically etched Au/Ag tips are used frequently. Among various methods for providing tips, the electrochemical etching method is considered as a suitable way to produce nice tips for TERS. The silver wire and gold wire are usually etched as tips, considering the resonance effect with different excitation wavelengths, as shown in Fig. 2b, c [47, 48, 51].

Besides, the substrate of TERS can be prepared in various ways, and the nanostructures are varied. For example, a novel starch-mediated photochemical reduction method can be applied to synthesis micrometer-sized gold nanoplates that have the combined properties of the size as micrometer scale and thickness as nanoscale. This method not only can provide various shapes of gold nanoplates but also can control the size range from a few micrometers to 100 μm. Through the preparation, only starch and sunlight are required instead of complicated chemical reactions. And, the detection of less than 100 target molecules can be investigated. What is more, the deposition of target molecules on the surface of Au substrate can be easier because of the self-assembly from Au-S bonding which can lead to a stronger enhanced hot spot between the Au surface and the metal tip. And, the flat surface makes it more usable for TERS (Fig. 3).

As to improve the stronger signals, the resonance frequency between the tip and the incident light needs to be considered, as well as the coupling efficiency. The former one can be modified by changing the shape and size of tip apex [40, 41, 53], as the latter one can be modified by grating coupled excitation on the tip shaft, as shown in Fig. 2d [49, 54].

Fig. 2 Scanning electron microscopy (SEM) images of **a** a silver-coated metalized cantilever tip, **b** a typical etched Ag tip, **c** a typical etched Au tip, and **d** a conical metallic tip with a grating coupler on the shaft, prepared by focused ion beam sputtering. Adapted from Ref [46–49], respectively
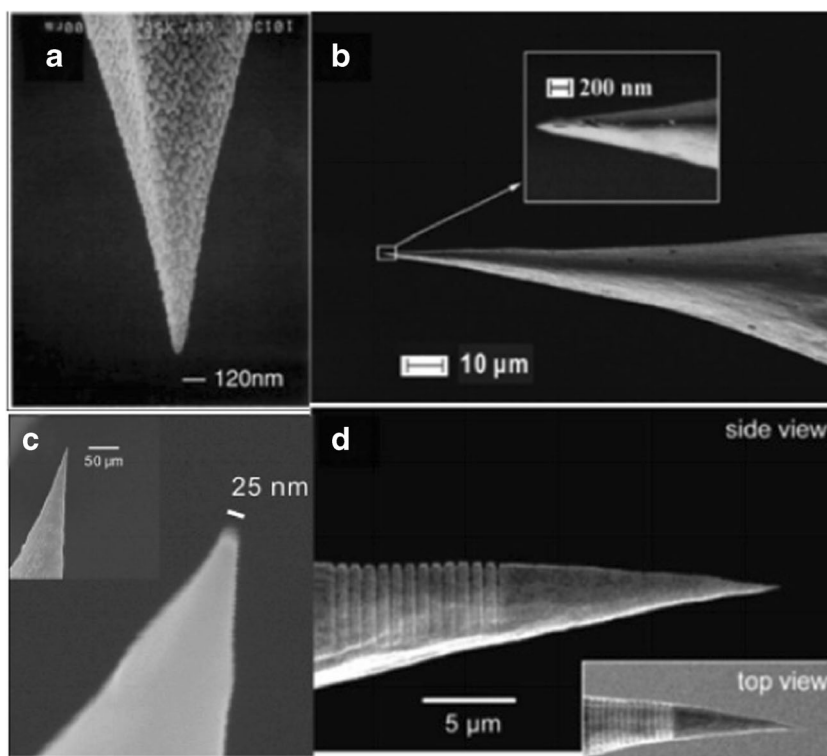
Optical Design

There is no doubt that the optical design is a critical part in the TERS setup. Through the setups, the excitation laser must be focused onto the tip apex and the Raman scattering signals collecting should be effective.

As shown in Fig. 1f, there are usually three geometry designs, as using bottom, side, and top illumination in the experimental setups. In a bottom illumination geometry, the light is focused on the tip apex through the substrate tightly. And, it is obvious that the sample and support frame should be transparent and not too thin [55]. However, the electric field enhancement is limited due to the limitation of polarization which is always being perpendicular to the tip axis [56]. Hartschuh et al. [57, 58] demonstrated that a radially polarized annular beam can lead to a higher field enhancement and can improve the image contrast in TERS.

Therefore, a side illumination setups are adopted in STM and SFM systems, and has the ability to excite a stronger electric field compared with the bottom illumination. Although it has a long working distance objective used to focus the laser, the excitation and collection efficiency are limited. While the laser power is increased to compensate for the decreased efficiency, the target molecules are easy to be damaged [9].

Top illumination can be used for transparent and opaque samples, usually used in AFM-TERS and SNOM-TERS, by combining the advantages of bottom and side illumination

setups. But, it requires a special tip or tip holder to avoid excitation and scattering light being blocked by the tip. And, because of its complexity of operation, a parabolic mirror TERS setup is designed and used successfully in STM-TERS. In this way, the excitation and collection efficiency can be largely improved, though the light is difficult to focus onto the tip apex.

The selection of illumination setups is depending on the configuration/structure of the SPM systems and on the samples of interest.

Sample Preparation

In TERS testing, a flat mica, glass slide, or silicon wafer are usually used [38, 59, 60]. When the tip and the substrate are both metal (gap-mode), instead, the substrate is not gold or silver film/single crystal usually, because of the cost of the gold and silver single crystals and the difficulty to obtain higher enhancement signals in an air atmosphere.

Normally, many researchers would use a 100–200 nm gold or silver film deposited in high vacuum on a mica or silicon wafer [22, 24, 61, 62]. The roughness of the prepared gold or silver film is similar to the arrays of metal tips which can lead to the LSPR effect. The electric field enhancement is generated by the coupling between the tip and the substrate. In this way, the Raman signal is strongly enhanced comparing with that on single-crystal substrates [63, 64].
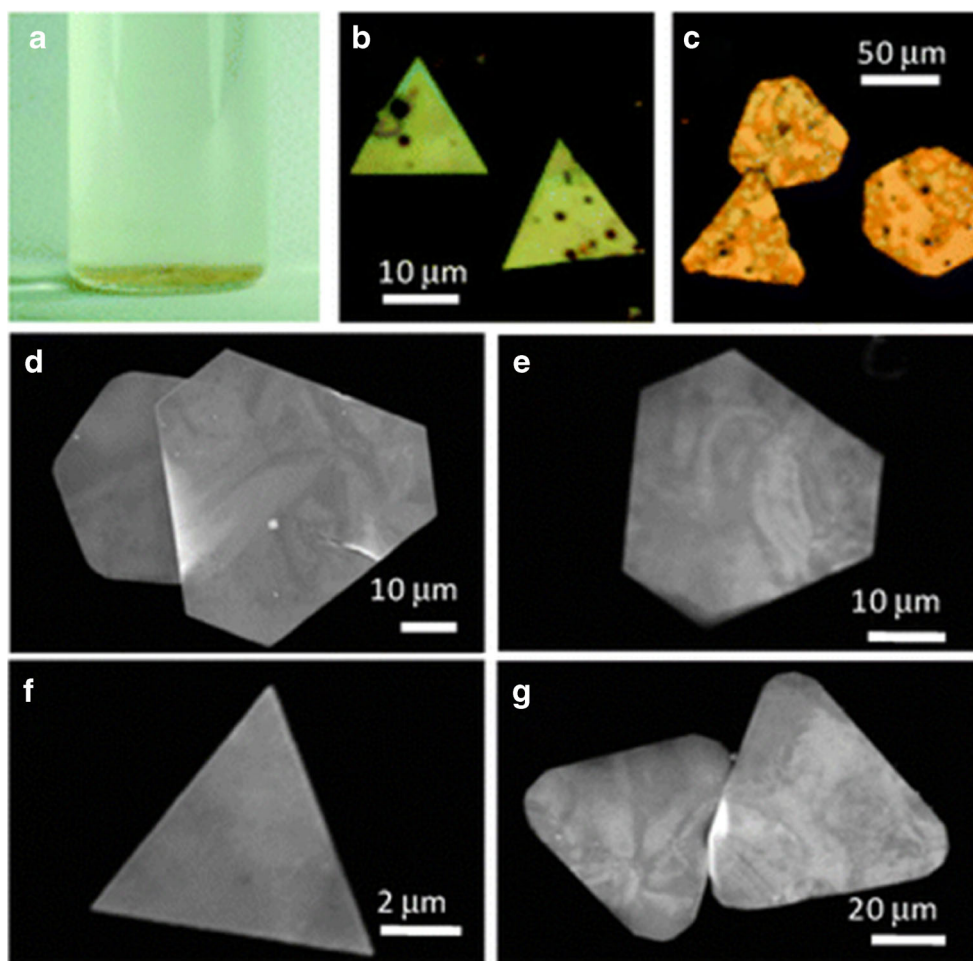
After preparing the substrates, it is also needed to discuss the way molecules adsorbed on the substrates. One is that to obtain a monolayer of self-assembled molecules via chemisorption, the substrates can be directly immersed into the molecule solutions [65, 66]. In another way, samples can be dispersed and physically adsorbed onto the substrates [59] by using the dying or spin coating method. However, it is difficult to obtain the topography of one molecule using SPM. Hence, by using the MBE method (molecular beam epitaxial method), only the target molecules on a clean single-crystal substrate can be obtained [20, 21, 23, 25]. In this way, the spectrum testing and topography measurements can be performed simultaneously.

Applications of TERS

Deep Ultraviolet TERS

In recent years, the technique of deep ultraviolet TERS (DUV-TERS) is advanced, due to its immeasurable potential in material sciences and bioscience [67–79]. Taguchi and co-workers first reported DUV-TERS in which the Si tip is coated by aluminum and the substrate is an aluminum film [76]. Aluminum (Al) has a big benefit in achieving SPR in the DUV region [75], down to a wavelength of 200 nm, and is widely used to investigate the design and applications of DUV-TERS. The following data are obtained theoretically by using finite-difference time-domain (FDTD) method, theoretically analyzed by Yang et al. [80].

The model used in the calculation is reduced to Fig. 4, while the optical data are taken from ref. [81].

When the tip is pure Al, various parameters are discussed. Figure 5a is investigated when the $r = 30$ nm and $d = 2$ nm. It indicates that the strong electromagnetic enhancement will appear ranges from 200 to 400 nm, as well as shows that when $\theta = 25°$, it will lead to the strongest enhancement. Figure 5b reveals that when t increases from 5 to 15 nm, the enhancement will increase sharply and blue shift. And then, when the t continued to increase, the factor of enhancement will grow gradually and tend to stabilize. Figure 5c shows that the value of optimal hemisphere (r) is better fixed in the range from 20 to 45 nm.
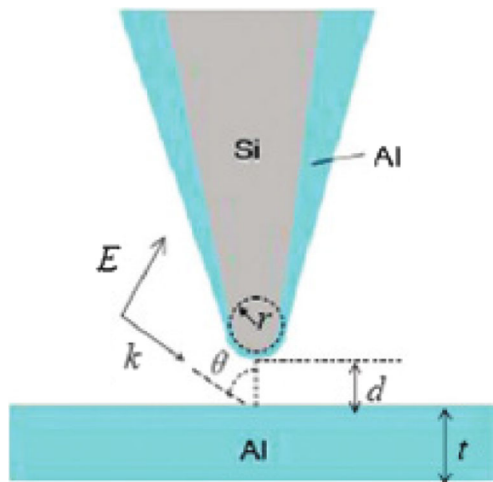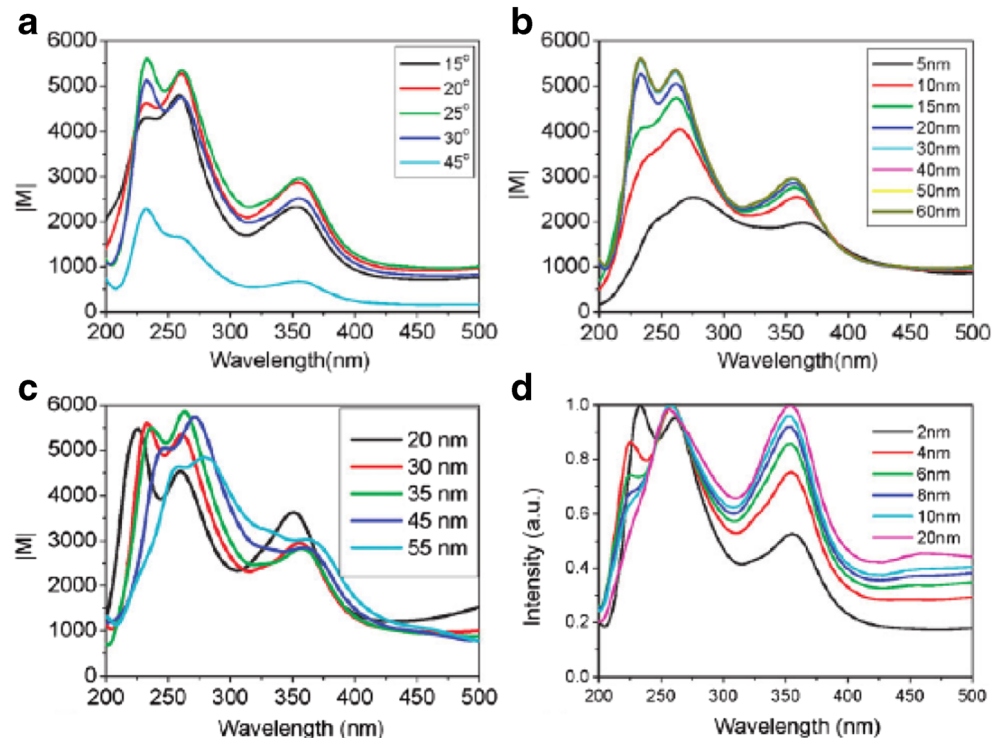
Fig. 4 The model of DUV-TERS in the calculations

And, the distance d is better hold on 2 nm, as shown in Fig. 5d. When $1\,nm \leq d \leq 2\,nm$, the hot spot is localized at the core of the gap. But, if d is too large, as well as too short, the electron tunneling transfer in the gap will lead to an unconvincing result.

When the silicon tip is coated by aluminum with different thickness, we can find out that $t = 40$ nm, $d = 2$ nm, and $r = 15$ nm with thickness ranges from 15 to 30 nm, is the best parameters (Fig. 6a). If the thickness of coated aluminum is larger than 15 nm, these two peaks shown in Fig. 6a will red shift; when the thickness is larger than 40 nm, the intensity will decrease gradually. Figure 6b shows that when the thickness of the substrate increased,

the factor of enhancement will grow obviously. However, when $t \geq 30$ nm, the enhancement will not grow obviously. As shown in Fig. 6c, when θ ranges from 15° to 25°, the intensity at 222 nm is improved; while θ grows continually, then the intensity will decrease indeed. So, the 25° is the suitable value of incident angle. Figure 6d shows that the intensity negatively correlated with the distance. It also reveals that in the core of the gap, we can obtain the strongest electromagnetic enhancements.

Figure 7 reveals that, which is obvious and easy to understand, the factor of enhancements would decrease gradually when the thickness of Al_2O_3 increased. Although the Al_2O_3 will decrease the SERS enhancement, it can provide an isolated layer to prevent the direct reaction between the aluminum tip and the target molecules, similar to shell-isolated nanoparticle-enhanced Raman spectroscopy (SHINERS) [82, 83].

In conclusion, the results about parameters help us better understand the mechanism of DUV-TERS, and to invent and improve the new technique about DUV-TERS.

HV-TERS

Introduction

The atmospheric TERS can obtain a spectral enhancement which is no better than traditional SERS (surface-enhanced Raman spectroscopy), so the HV system is needed to gain more information. In the high-vacuum environment, the

Fig. 5 **a** The incident angle (θ),. **b** The thickness of the substrate (t). **c** The hemisphere radius (r). **d** The distance (d)-dependent surface plasmon enhancements of DUV-TERS, where $|M| = |E_{local}/E_{in}|$, and E_{local} and E_{in} are local and incident electric fields, respectively

Fig. 6 **a** The hemisphere radius (*r*). **b** The thickness of the substrate (*t*). **c** The incident angle (*θ*) , and. **d** The distance (*d*)-dependent surface plasmon enhancements of DUV-TERS, where the tip is an Al-coated silicon tip
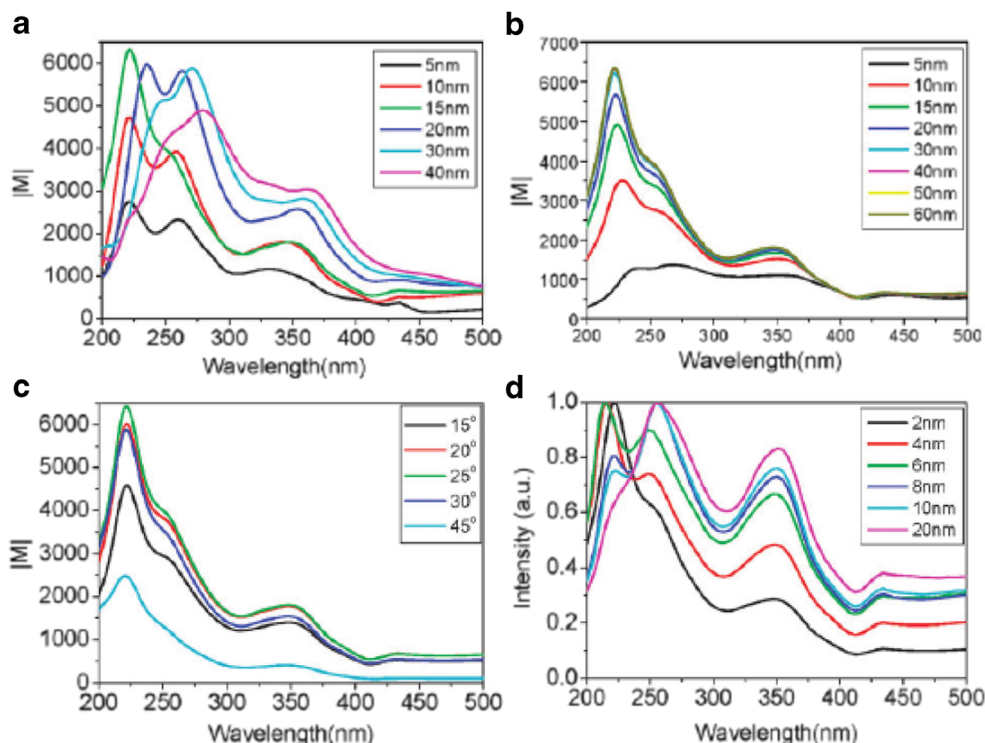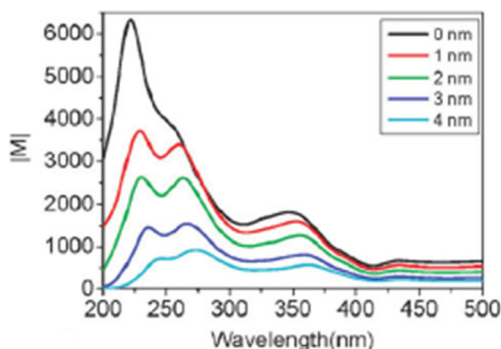

optical spectral and spatial resolutions are enormous enhanced because of the tunneling current and field gradient effect [84], compared with scanning near-field optical microscopy. Hence, the experiments performed in HV-TERS lead to some additional non-linear effect, compared with atmospheric TERS, such as simultaneously active infrared and Raman vibrational modes and Fermi resonance. To study the basic surface more accurately, as well as the ultrapure environment, the high spatial and spectral resolution are required.

By the system, Sun [24] et al. designed an Au single-crystalline film for TERS in the MBE chamber (in situ) with a mica substrate. Instead, the sample can be prepared and loaded by the fast loading chamber (ex situ). And, the entire STM scanner is placed inside the HV chamber, and two magnetic mechanical robot hands are used to transfer the samples;

Fig. 7 The thickness of the Al_2O_3 layer-dependent electromagnetic field at *y* = 25°, where the thickness of Al coated on the silicon tip is 15 nm, *t* = 40 nm, where the thickness of Al_2O_3 is included in the thickness of Al

in this way, the high vacuum becomes easier to obtain by avoiding frequent opening. Furthermore, similar HV-TERS setups have been built by other groups. For example, in Pettinger's setup [85], all the Raman optics and STM are contained in the high-vacuum chamber. In this setup, a long time for alignment is required and it is difficult to replace the filter because all the optical components are inside the chamber when the incident laser needs to be changed. In Van Duyne's setup [86], all the optics are outside the chamber. Hence, it needs a long working distance for the objective, and the laser spot is hard to focus tightly because the small NA (numerical aperture). And, the Raman signal with high intensity is hard to be obtained (Fig. 8).

Adapted from [87]

Compared with above setups, Sun's setup allows convenient access of optics with a large objective, and the samples can be prepared in situ without contamination by air, as samples are prepared ex situ by all the setups mentioned above. In another word, the high vacuum makes sure that the experiment runs in a pure condition to decrease the contamination of the sample. Besides, the STM tip-substrate gap is kept in a pure tunneling state.

Surface Catalytic Reactions on HV-TERS

Localized surface plasmons (LSPs) that excited on the surfaces of noble metal nanoparticle can decay into "hot electrons", of which the energy is between the Fermi and vacuum energy level [88]. When the "hot" electrons scatter
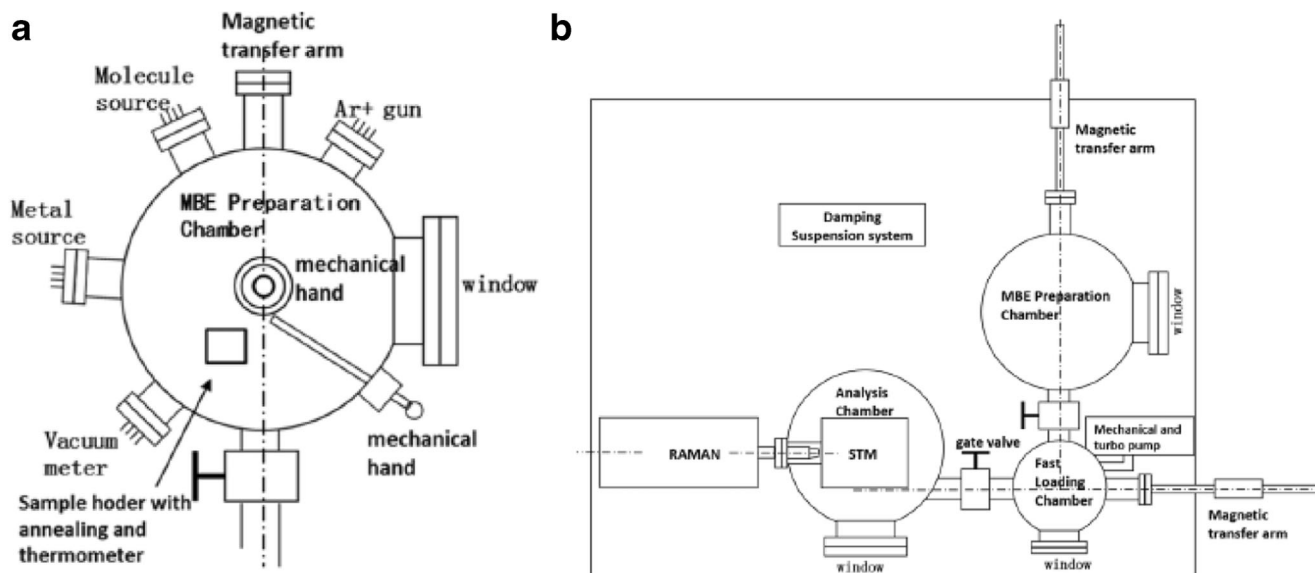
Fig. 8 **a** Schematic diagram of the MBE chamber. **b** Schematic illustration of the HV-TERS system built by Sun's group [24]

into an excited state, the "plasmon-driven reaction" will be occurred by decreasing the activation energy [89–91]. By using several kinds of SERS, the plasmon-driven reactions can be tracked at nanoscale [92, 93], such as single molecule SERS, graphene-mediated surface-enhanced Raman scattering (G-SERS) [94–96], and remotely excited SERS [97–99]. The high spatial resolution and controllability make TERS an

ideal tool for studying plasmon-driven reactions. In 2012, plasmon-driven reactions are first revealed by TERS [21, 100].

With the HV-TERS system built by Sun's group, the plasmon-driven chemical reactions can be monitored in situ. In the TERS setup, the distance between the substrate and the tip can be well controlled by STM (Table 1).

Table 1 Parameters and comparison of the three HV-TERS systems

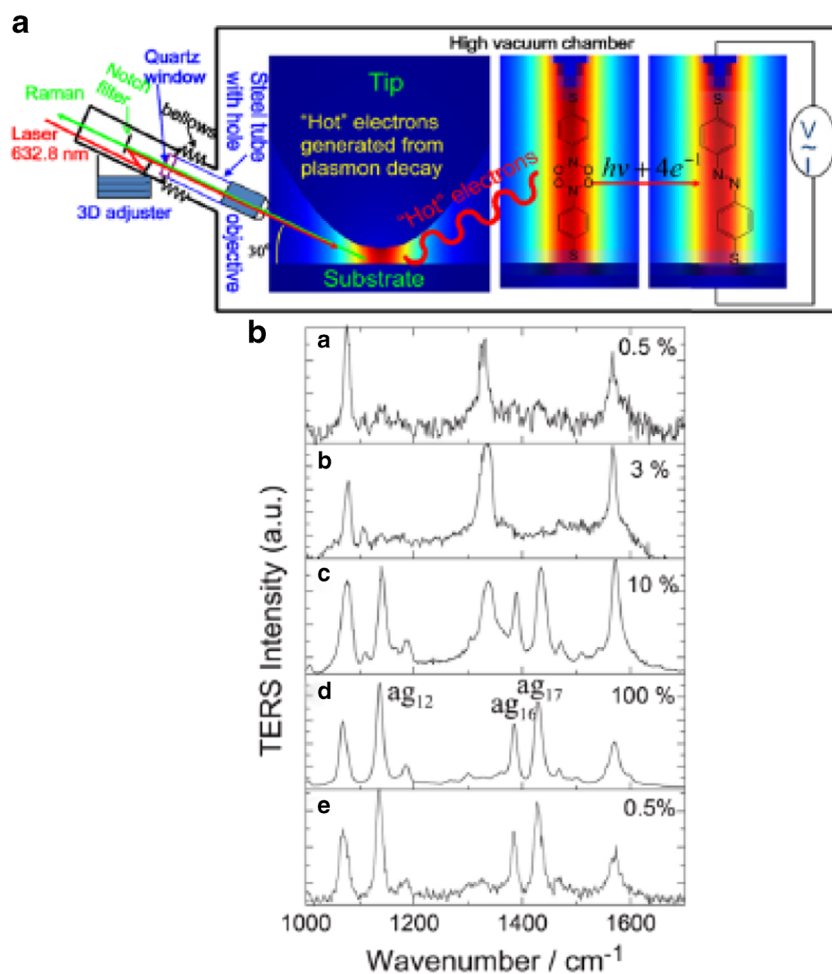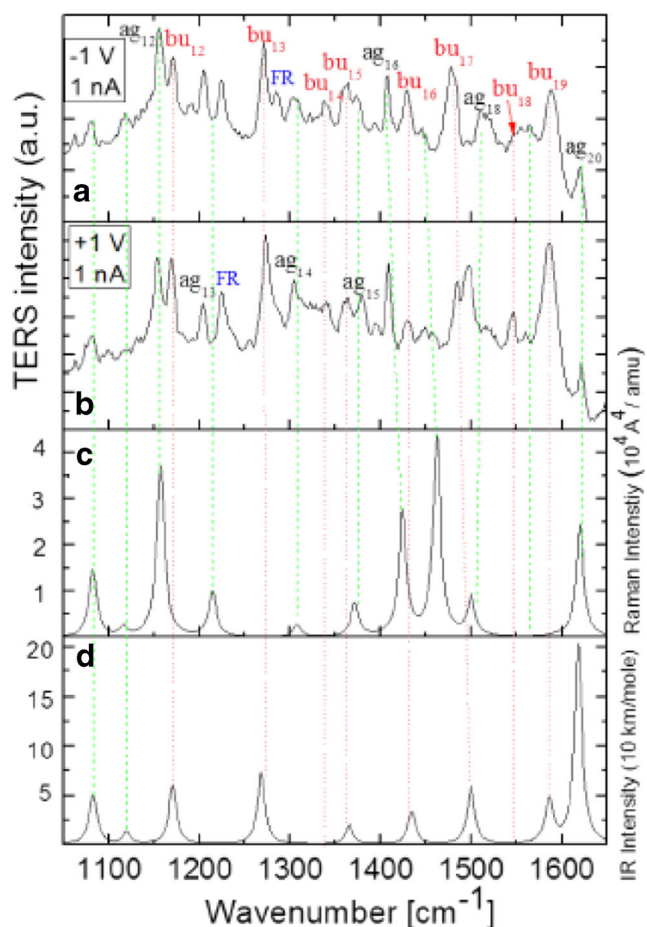| Configuration	All optical components inside the chamber[17]	All optical components outside the chamber[20]	Objective inside and other optics outside the chamber (our system)
Objective	Parabolic mirror (4 mm)	Long work distance lens (~200 mm)	Middle work distance objective (10 mm)
NA of objective	0.65 (21°–90°)	~0.01	0.5
Planapochromat (P/F)	(No/yes)	No	Yes
Vacuum	10^{-8} Pa	6.6×10^{-9} Pa	10^{-7} Pa
Laser	633 nm	633 nm	633 nm
Laser spot	300 nm	60×40 μm	~1 μm
Laser and collection path efficiency	Low (55–60% loss)	Very low (low NA, widows, and big spot)	High (~20% loss)
Tip curvature	25 nm	100 nm	25 nm
STM spatial resolution	0.1 nm (transvers)	0.1 nm (transvers)	0.1 nm (transvers)
Raman spectral resolution		15	0.5 cm^{-1}
Raman spatial resolution	15 nm		30 nm
Polarization control	No, fixed	Yes	Yes
Atomic resolution	Yes	Yes	Yes
Alignment	Whole complex optical components inside the chamber	Two light paths (excitation and collection) outside the chamber	One light path outside the chamber
In situ measurement	No	No	Yes
Flexibly modification of optical path with keeping vacuum	No	Yes	Yes
Preparation chamber	No	No	Yes

As shown in Fig. 9, the mechanism of the "plasmon-driven" chemical reactions of 4-nitrobenzenethiol (4NBT) to DMAB can be investigated by increasing the intensity of plasmon, which strongly depends on the intensity of incident laser. The HV-TERS Spectra of 4NBT at a low power of incident laser were studied as shown in Fig. 9b. When the intensity of incident laser was increased (still lower than 3% of the full laser power), first of all, no change of the TERS peaks was obtained (Fig. 9b (b)). The main peaks at 1073, 1336, and 1587 cm^{-1} were all attributed to 4NBT [101]. When the intensity of incident laser is larger than 3%, three new peaks were appeared due to the process (4NBT dimerize to DMAB) by plasmonic catalysis. The strongly enhanced 1432 cm^{-1} peak is related to the –N = N– stretching vibrational mode. As shown in Fig. 9b (c), the characteristic peak at 1336 cm^{-1} of 4NBT for the –NO$_2$ stretching mode is still obtained, as the 4NBT and DMAN are both existed. When the laser intensity was increased to its original intensity, the fingerprint vibrational peak of 4NBT almost disappeared, indicating that the 4NBT were dimerized to DMAB mostly (Fig. 9b (b)). As shown in Fig. 9b (e), a molecular

changed has occurred compared with Fig. 9b (a), as even when the incident laser power was reduced to 0.5%, same as the intensity was used in Fig. 9b (a). This experiment reveals that the plasmon-driven reaction of 4NBT to DMAB will appear at a strong plasmon intensity and the reaction is irreversible. Furthermore, in the STM-based HV-TERS, by modifying the tunneling current and bias voltage, the intensity of plasmon in the nanogap can be well controlled. Hence, a new way to control chemical reactions is obtained.

As the 4NBT can be reduced to DMAB in the HV-TERS, the PATP can be dimerized to DMAB by plasmon-driven oxidized reaction [84, 89, 102–105]. Figure 10 shows a HV-TERS study of PATP molecules on an Au substrate (related positions are pointed by arrows on the TERS mapping). The TERS spectrum of PATP is different form the SERS and normal Raman spectra of PATP. The additional peaks that emerge in SERS spectrum are due to the plasmon-assisted chemical reaction. But, in the HV-TERS system, there are more Raman peaks than in SERS spectrum (Fig. 10a, b). The increased number of peaks has been attributed to the gradient-field effect in HV-TERS-induced molecular quadrupole transitions [106,

Fig. 9 **a** Schematic diagrams of the plasmon-driven chemical reaction measured in HV-TERS and the laser intensity-controlled dynamics of plasmon-driven chemical reactions. **b** TERS spectra at laser powers of 0.5% (*a*), 3% (*b*), 10% (*c*), 100% (*d*), and 0.5% (*e*) at a bias voltage of 1 V and current of 1 nA. Assignment of the vibrational modes of A$_{g12}$, A$_{g16}$, and A$_{g17}$ for dimercaptoazobenzene (DMAB) (*d*). Reproduced with permission from Sun et al. [21]

Fig. 10 TERS peaks of *p*-aminothiophenol (PATP) under experimental conditions of 1 nA current and **a** −1 V and **b** +1 V bias voltage. **c** Simulated Raman and **d** IR spectra of DMAB, where the wave number is scaled by 1.014. Adapted from Ref [61]

which is frequently observed in IR or Raman spectra of the symmetric triatomic molecules. Hence, the high vacuum can be used for obtaining FR in the more complicated molecules and improving the image resolution.

In conclusion, to obtain a pure environment, the influence of air, water, or others from the atmosphere should be avoided by a HV system. And, it guarantees sub-molecular resolution imaging of target molecules for SPM to perform the in situ topographical and spectral imaging simultaneously. The HV-TERS provides an effective way to analyze the nature of plasmon-driven reactions and the basic mechanism of molecules and molecular interactions.

Plasmonic Scissors for Molecular Design on TERS

As shown above, surface plasmon can assist molecular synthesis, such as synthesis of DMAB from PATP and 4NBT revealed by SERS. But, all of these experiments are plasmon-assisted synthesis reactions. Can dissociation of DMAB be explained exhaustively in SERS? First problem we must face to is that the hot electrons generated from plasmon decay can be easily quenched in ambient SERS. The HV system can be used for performing the dissociation process by prohibiting the quenching of hot electrons. Hence, HV-TERS is considered as a useful tool for realizing surface catalytic reactions by controlling selective dissociation, as a plasmonic scissor.

The hot site can be created by the metal tip in HV-TERS due to the excited strong surface plasmon resonances (SPR). And, when the plasmon decays, more hot electrons are created at the apex of the tip. The HV system provides ample space to protect the hot electrons from quenching, and the reaction barrier for dissociation can be decreased [108, 109].
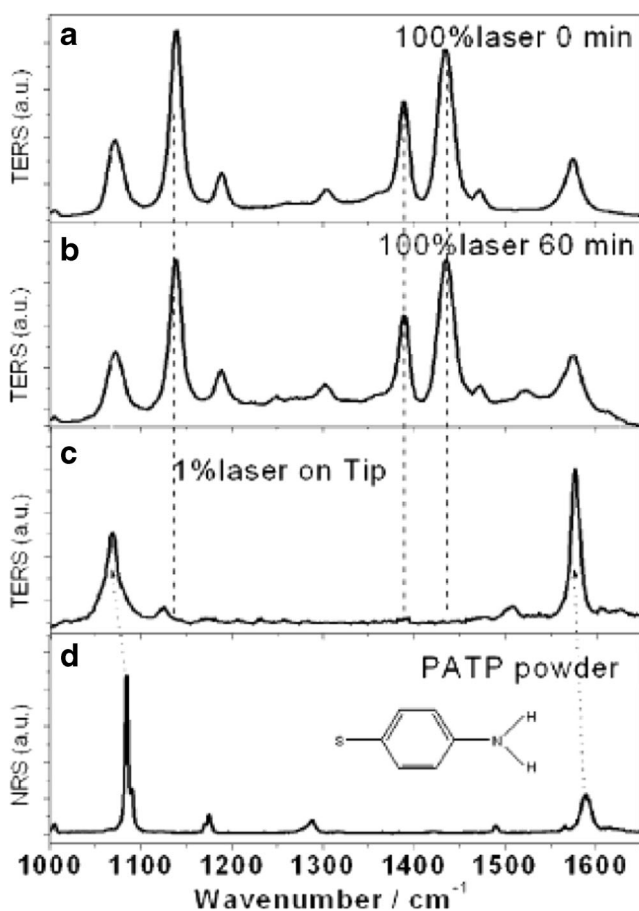
As have been introduced above, DMAB can be synthesized from PATP and 4BNT. In the other way, the process of dissociated fragments dimerized back to DMAB is very quick through the –N = N– bond. The dissociation cannot be obtained when the dissociation is competing with synthesis [110]. But by tuning the pH value, the dimerization of dissociated radical fragment can be prevented, which is already confirmed in SERS (Fig. 11) [111, 112].

107]. Considering the simulated Raman spectrum (Fig. 10c), all the Raman-active symmetric Ag vibrational modes in Fig. 10a, b can be assigned. Noted that most of the remaining Raman peaks in Fig. 10a, b can be assigned as IR-active asymmetric Bu modes, compared with the simulated IR spectrum (Fig. 10d).

However, this phenomenon has not been observed in atmospheric TERS experiments. The Raman-active A_{g13} mode splits into two Raman peaks due to Fermi resonance (FR)

Fig. 11 Schematic of HV-TERS, mechanism of dissociation by plasmonic scissors, and the product control by means of different pH values
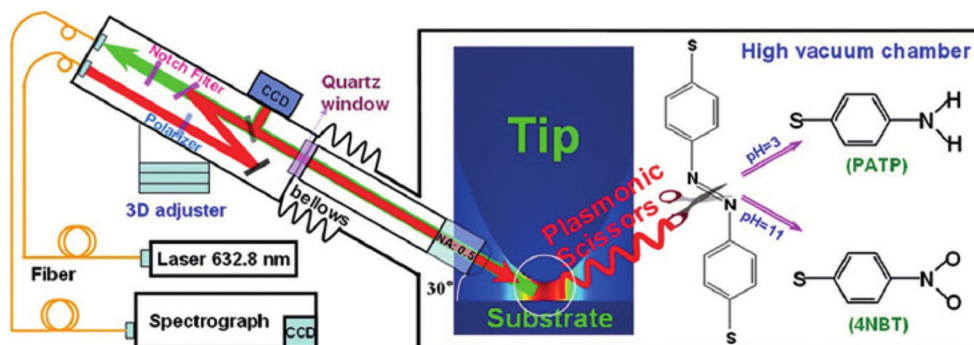
Under acidic condition, DMAB in the gap could be excited at original intensity of laser (2 mW), and the time span of TERS ranges from 0 to 60 min. And, with the help of acidic condition, if the –N = N– bond of DMAB was broken, the dissociated fragments would be located on the tip or the substrate. But, after 60 min, there is no significant change of DMAB by TERS. When the laser power is decreased to 1% (20 µW) and focused on the tip, the measured TER spectrum (Fig. 12c) is significantly different from Fig. 12a. The A_{g17} mode of DMAB disappearance is completely due to the selectively dissociated –N = N– bond.

After the DMAB molecule was dissociated selectively, PATP can be obtained from the attachment between the radical fragment and the hydrogen-ions. Similarly, the 4BNT can be produced by the attachment between oxygen-ions and fragments. By measuring the normal Raman spectral of PATP power (Fig. 12d), it reveals that PATP cannot convert to DMAB at a weak plasmon, which is not enough to reach the reaction threshold and confirm the above assumption.
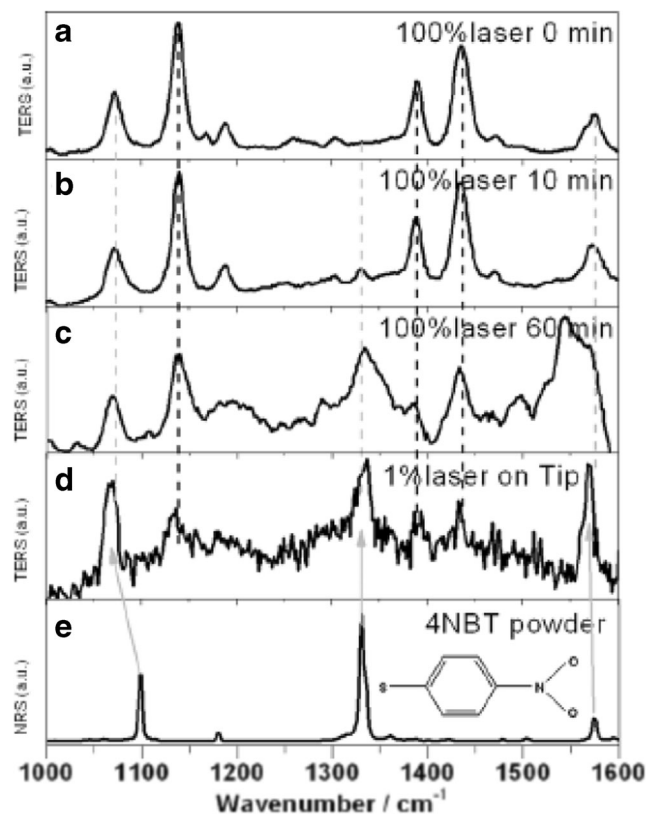
Analogously, DMAB under alkaline condition (Fig. 13) is also measured by TERS. Figure 13a–c shows the spectra measured at 0, 10, and 60 min with 100% of laser. In Fig. 13b, after 100% laser excitation for 10 min, a weak vibrational peak appears. And at 60 min, it obviously increased and the –N = N– stretching mode at 1433 cm^{-1} is decreased obviously in Fig. 13c. Figure 13d is measured on the substrate which is retracted from the experiment of Figure 13c, and 1% laser intensity is applied. The Raman spectrum is like the normal Raman spectrum of 4NBT powder in Fig. 13d. Hence, the assumptions above are confirmed.

Figure 14 shows the process of pH-controlled products of the dissociation by plasmonic scissors in HV-TERS. With the help of laser, the reaction energy can be excited to be higher or close to the dissociation. Hence, the hot electrons can use its high kinetic energy to selectively dissociate the –N = N– bond [113].

In conclusion, to obtain the selective dissociation of DMAB needs three process. First of all, strong plasmonic scissors need to be produced due to SPR. Secondly, the attachment between the substrate and ions is necessitated for a decreased reaction barrier. Lastly, the weak plasmons excited by a low incident laser are required to obtain Raman signals and prevent the backwards synthetic process.

Fig. 12 Experimental TER (acidic conditions) and NR spectra. TER spectra of DMAB at **a** 0 and **b** 60 min. **c** TER spectrum on tip with weak excitation after strong excitation for 60 min. **d** (normal Raman spectrum) NRS of PATP powder

Fig. 13 Experimental TER (alkaline conditions) and NR spectra. TER spectra of DMAB at **a** 0, **b** 10, and **c** 60 min. **d** TER spectrum on tip with weak excitation after strong excitation for 60 min. **e** NRS of 4NBT powder

Fig. 14 The process of pH control of products of the dissociation by plasmonic scissors in HV-TERS. **a** Scheme of reaction paths, in accordance with experimental results. **b** Dynamic process of chemical reaction under acidic conditions
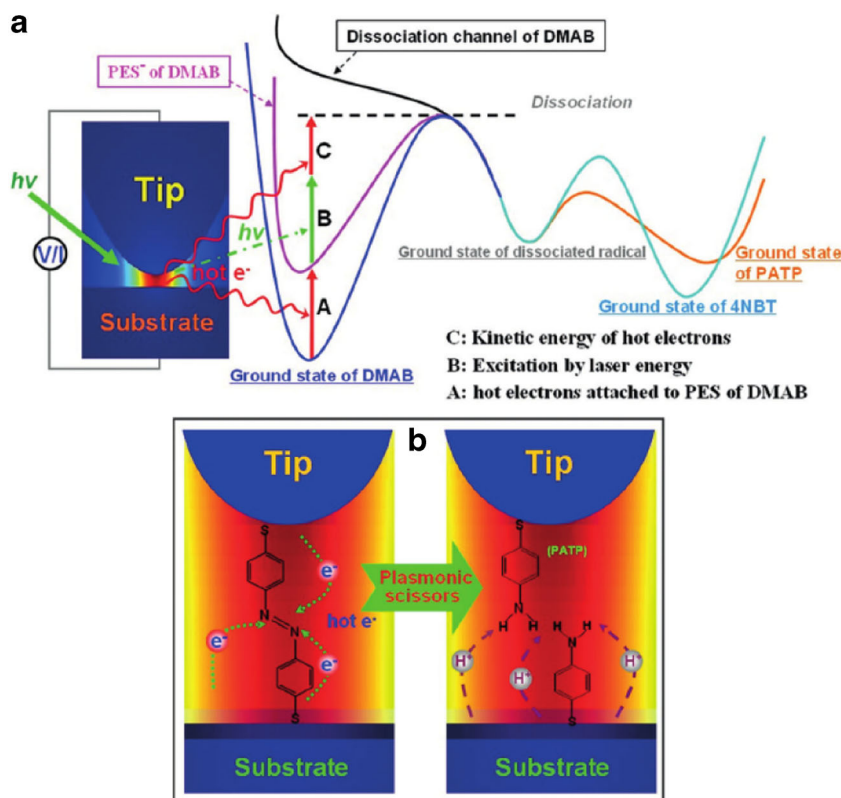
HV-TERS has many merits; above all, it provides a pure environment for SPs. Moreover, the intensity of plasmon can be tuning easily, such as tunneling current, changing bias voltage and intensity of plasmon.

In this way, plasmonic scissors can be successfully applied by controlling the pH in HV-TERS.

Plasmonic Gradient Effects on TERS

As shown in the above chapter, there is a lot of experimental evidence of the breakdown of Raman selection rules in HV-TERS.

Because of the strong tip-enhanced near-field gradient effects, the molecular Raman-active, IR-active, and overtone modes can be observed in situ simultaneously.

The Hamiltonian for Raman spectra of a molecule placed in an inhomogeneous electromagnetic field can be written as [114]

$$H = H_0 + H_1 + H_2$$
$$= \alpha_{\alpha\beta}E_\beta E_\alpha + \frac{1}{3}A_{\alpha,\beta\gamma}\frac{\partial E_{\beta\gamma}}{\partial r}E_\alpha + \frac{1}{3}\left(A_{\gamma,\alpha\beta}E_\gamma + C_{\alpha\beta,\gamma\delta}\frac{\partial E_{\gamma\delta}}{\partial r}\right)\frac{\partial E_{\alpha\beta}}{\partial r} + \dots$$

where $\alpha_{\alpha\beta}$, $A_{\alpha,\beta\gamma}$, and $C_{\alpha\beta,\gamma\delta}$ are the electric dipole–dipole polarizability, the electric dipole–quadrupole polarizability and the electric quadrupole–quadrupole polarizability, and E_α and $\frac{\partial E_{\alpha,\beta\gamma}}{\partial r}$ are the external electric field and external electric field gradient, respectively [115–118].

Almost all the studies on TERS are mainly focused on the diagonal part in the equation and the configuration of the molecule adsorbed on the substrate. Hence, the tip-enhanced resonance coupling (TERC) remains to be explored in HV-TERS experimentally and theoretically. The unexpected "additional" Raman peaks in linear harmonic TERS have been attributed to molecular anharmonicity and can provide vast ultrasensitive vibrational information for chemical analysis.

Figure 15 is the distance dependent ratio of $\frac{\partial E_{\beta\gamma}}{\partial r}\frac{\partial E_{\beta\gamma}}{\partial r}/E_\beta E_\alpha$, while the second and the third terms are
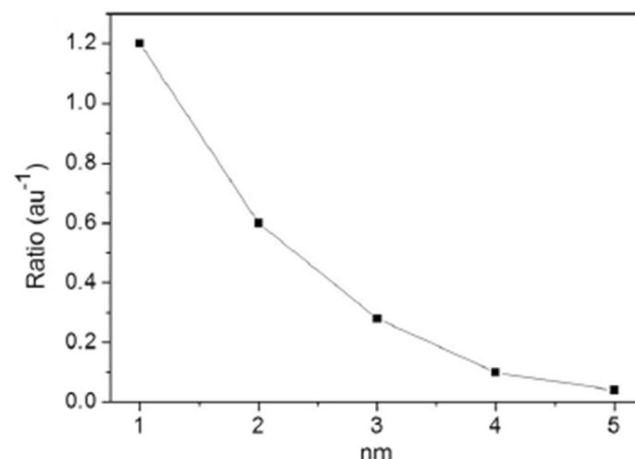
Fig. 15 Distance dependent ratio of $\frac{\partial E_{\beta\gamma}}{\partial r}\frac{\partial E_{\beta\gamma}}{\partial r}/E_\beta E_\alpha$. Noted that the unit of electric field intensity is V/m, and the unit of electric field gradient is V/m/au, where au is atomic unit

considered in the calculations. It reveals that the ratio is significantly decreased, and when the distance is larger than 5 nm, the near field gradient effects can be ignored basically [57].

Summary

With the help of SPM, the coupling between tip and substrate of TERS can excite strong surface plasmons to induce surface chemical reaction and enhance the spatial resolution, even the unexpected additional peaks appeared. In more detail, hot electrons with high kinetic energy can be created by the decay of surface plasmons. Then, the reaction barrier was decreased due to that. Stronger plasmon resonance that generated from the stronger laser intensity can produce a higher density of hot electrons with a higher kinetic energy. When the hot electrons jump to the unoccupied resonant energy level of chemical reactants, the equilibrium potential energy surface changed to a temporal negative ion situation of the composite adsorbed molecules that lead to the plasmon-driven chemical reaction. Due to that, the design of molecules and selectively dissociation of specific bond can be produced. In this way, it indicates that TERS has an immeasurable potential.

References

1. Shiohara A, Wang Y, Liz-Marzán LM (2014) Recent approaches toward creation of hot spots for SERS detection. J Photochem Photobiol C: Photochem Rev 21:2–25
2. Yang X, Yu H, Guo X, Ding Q, Pullerits T, Wang R, Zhang G, Liang W, Sun M (2017) Plasmon-exciton coupling of monolayer MoS_2-Ag nanoparticles hybrids for surface catalytic reaction. Mater Today Energy 5:72–78
3. Ding Q, Chen M, Fang Y, Zhang Z, Sun M (2017) Plasmon-driven Diazo coupling reactions of p-Nitroaniline via $-NH_2$ or $-NO_2$ in atmosphere environment. J Phys Chem C 121(9):5225–5231
4. Albrecht MG, Creighton JA (1977) Anomalously intense Raman spectra of pyridine at a silver electrode. J Am Chem Soc 99:5215–5217
5. Wessel J (1985) Surface-enhanced optical microscop. J Opt Soc Am B 2:1538–1541
6. Hayazawa N, Inouye Y, Sekkat Z, Kawata S (2000) Metallized tip amplification of near-field Raman scattering. Opt Commun 183:333–336
7. Pettinger B, Picardi G, Schuster R, Ertl G (2000) Surface enhanced Raman spectroscopy: towards single Moleculer spectroscopy (E). Electrochemistry-TOKYO 68(12):942–949
8. Stockle RM, Suh YD, Deckert V, Zenobi R (2000) Nanoscale chemical analysis by tip-enhanced Raman spectroscopy. Chem Phys Lett 318:131–136
9. Moskovits M (1985) Surface-enhanced spectroscopy. Rev Mod Phys 57(3):783–826
10. Metiu H, Dos P (1984) Rev Phys Chem 35:507–536
11. Xu HX, Bjerneld EJ, Kall M, Borjesson L (1999) Spectroscopy of single hemoglobin molecules by surface enhanced Raman scattering. Phys Rev Lett 83:4357–4360
12. Otto A, Mrozek I, Grabhorn H, Akemann W (1992) Surface-enhanced Raman scattering. J Phys Condens Matter 4:1143–1212
13. Xia L, Chen M, Zhao X, Zhang Z, Xia J, Xu H, Sun M (2014) Visualized method of chemical enhancement mechanism on SERS and TERS. J Raman Spectrosc 45(7):533–540
14. Kneipp K, Wang Y, Kneipp H, Perelman LT, Itzkan I, Dasari R, Feld MS (1997) Single molecule detection using surface-enhanced Raman scattering (SERS). Phys Rev Lett 78:1667–1670
15. Wang D, Zhu W, Best MD, Camden JP, Crozier KB (2013) Directional Raman scattering from single molecules in the feed gaps of optical antennas. Nano Lett 13(5):2194–2198
16. Lim DK, Jeon KS, Kim HM, Nam JM, Suh YD (2010) Nanogap-engineerable Raman-active nanodumbbells for single-molecule detection. Nat Mater 9(1):60–67
17. Xie C, Mu C, Cox JR, Gerton JM (2006) Tip-enhanced fluorescence microscopy of high-density samples. Appl Phys Lett 89(14):143117
18. Ma Z, Gerton JM, Wade LA, Quake SR (2006) Fluorescence near-field microscopy of DNA at sub-10 nm resolution. Phys Rev Lett 97(26):260801
19. Dong ZC, Guo XL, Trifonov AS, Dorozhkin PS, Miki K, Kimura K, Yokoyama S, Mashiko S (2004) Vibrationally resolved fluorescence from organic molecules near metal surfaces in a scanning tunneling microscope. Phys Rev Lett 92(8):086801
20. Steidtner J, Pettinger B (2008) Tip-enhanced Raman spectroscopy and microscopy on single dye molecules with 15 nm resolution. Phys Rev Lett 100(23):236101
21. Sun M, Zhang Z, Zheng H, Xu H (2012) In-situ plasmon-driven chemical reactions revealed by high vacuum tip-enhanced Raman spectroscopy. Sci Rep 2:647
22. Zhang R, Zhang Y, Dong ZC, Jiang S, Zhang C, Chen LG, Zhang L, Liao Y, Aizpurua J, Luo Y, Yang JL, Hou JG (2013a) Chemical mapping of a single molecule by plasmon-enhanced Raman scattering. Nature 498(7452):82–86
23. Klingsporn JM, Jiang N, Pozzi EA, Sonntag MD, Chulhai D, Seideman T, Jensen L, Hersam MC, Van Duyne RP (2014) Intramolecular insight into adsorbate-substrate interactions via low-temperature, ultrahigh-vacuum tip-enhanced Raman spectroscopy. J Am Chem Soc 136(10):3881–3887
24. Fang YR, Zhang ZL, Sun MT (2016) High vacuum tip-enhanced Raman spectroscope based on a scanning tunneling microscope. Rev Sci Instrum 87:033104
25. Domke KF, Pettinger B (2010) Studying surface chemistry beyond the diffraction limit: 10 years of TERS. ChemPhysChem 11(7):1365–1373
26. Bailoa E, Deckert V (2008) Tip-enhanced Raman scattering. Chem Soc Rev 37:921–930
27. Langeluddecke L, Singh P, Deckert V (2015) Exploring the Nanoscale: fifteen years of tip-enhanced Raman spectroscopy. Appl Spectrosc 69(12):1357–1371
28. Nie S, Emory SR (1997) Probing single molecules and single nanoparticles by surface-enhanced Raman scattering. Science 275(21):1102–1106
29. Jiang N, Foley ET, Klingsporn JM, Sonntag MD, Valley NA, Dieringer JA, Seideman T, Schatz GC, Hersam MC, Van Duyne RP (2012) Observation of multiple vibrational modes in ultrahigh vacuum tip-enhanced Raman spectroscopy combined with molecular-resolution scanning tunneling microscopy. Nano Lett 12(10):5061–5067

30. Zhang Z, Sheng S, Wang R, Sun M (2016) Tip-enhanced Raman spectroscopy. Anal Chem 88(19):9328–9346

31. Rasmussen A, Deckert V (2006) Surface- and tip-enhanced Raman scattering of DNA components. J Raman Spectrosc 37(1–3):311–317

32. Bailo E, Deckert V (2008) Tip-enhanced Raman spectroscopy of single RNA strands: towards a novel direct-sequencing method. Angew Chem Int Ed Engl 47(9):1658–1661. doi:10.1002/anie.200704054

33. Wood BR, Bailo E, Khiavi MA, Tilley L, Deed S, Deckert-Gaudig T, McNaughton D, Deckert V (2011) Tip-enhanced Raman scattering (TERS) from hemozoin crystals within a sectioned erythrocyte. Nano Lett 11(5):1868–1873

34. Pozzi EA, Sonntag MD, Jiang N, Klingsporn JM, Hersam MC, Van Duyne RP (2013) Tip-enhanced Raman imaging: an emergent tool for probing biology at the Nanoscale. ACS Nano 7:885–888

35. Treffer R, Bohme R, Deckert-Gaudig T, Lau K, Tiede S, Lin X, Deckert V (2012) Advances in TERS (tip-enhanced Raman scattering) for biochemical applications. Biochem Soc Trans 40(4):609–614

36. Karrai K, Grober RD (1995) Piezoelectric tip-sample distance control for near field optical microscopes. Appl Phys Lett 66:1842–1844

37. Rensen WHJ, van Hulst NF, Kämmer SB (2000) Imaging soft samples in liquid with tuning fork based shear force microscopy. Appl Phys Lett 77(10):1557–1559

38. Kharintsev SS, Hoffmann GG, Dorozhkin PS, Gd W, Loos J (2007) Atomic force and shear force based tip-enhanced Raman spectroscopy and imaging. Nanotechnology 18(31):315502

39. Rodriguez RD, Sheremet E, Muller S, Gordan OD, Villabona A, Schulze S, Hietschold M, Zahn DR (2012) Compact metal probes: a solution for atomic force microscopy based tip-enhanced Raman spectroscopy. Rev Sci Instrum 83(12):123708

40. Stadler J, Schmid T, Zenobi R (2012) Developments in and practical guidelines for tip-enhanced Raman spectroscopy. Nano 4(6):1856–1870

41. Pettinger B, Domke KF, Zhang D, Picardi G, Schuster R (2009) Tip-enhanced Raman scattering: influence of the tip-surface geometry on optical resonance and enhancement. Surf Sci 603(10–12):1335–1341

42. Jain P, Yeo BS, Stadler J, Schmid T, Zenobi R, Zhang WH (2009) Tip-enhanced Raman spectroscopy – its status, challenges and future directions. Chem Phys Lett 472(1–3):1–13

43. Khiavi MA, Wood BR, Talemi PH, Downes A, Mcnaughton D, Mechler A (2012) Exploring the origin of tip-enhanced Raman scattering; preparation of efficient TERS probes with high yield. J Raman Spectrosc 43(2):173–180

44. Kharintsev SS, Hoffmann GG, Fishman AI, Salakhov MK (2013a) Plasmonic optical antenna design for performing tip-enhanced Raman spectroscopy and microscopy. J Phys D Appl Phys 46(14):145501

45. Zhang MQ, Wang R, Zhu ZD, Wang J, Tian Q (2013b) Experimental research on the spectral response of tips for tip-enhanced Raman spectroscopy. J Opt 15(5):055006

46. Hayazawa N, Inouye Y, Sekkat Z, Kawata S (2001) Near-field Raman scattering enhanced by a metallized tip. Chem Phys Lett 335:369–374

47. Zhang WH, Yeo BS, Schmid T, Zenobi R (2007) Single molecule tip-enhanced Raman spectroscopy with silver tips. J Phys Chem C 111:1733–1738

48. Xu G, Liu Z, Xu K, Zhang Y, Zhong H, Fan Y, Huang Z (2012) Constant current etching of gold tips suitable for tip-enhanced Raman spectroscopy. Rev Sci Instrum 83(10):103708

49. Ropers C, Neacsu CC, Elsaesser T, Albrecht M, Raschke MB, Lienau C (2007) Grating-coupling of surface Plasmons onto metallic tips: a Nanoconfined light source. Nano Lett 7(9):2784–2788

50. Downes A, Salter D, Elfick A (2006) Heating effects in tip-enhanced optical microscopy. Opt Express 14:5216–5622

51. Ren B, Picardi G, Pettinger B (2004) Preparation of gold tips suitable for tip-enhanced Raman spectroscopy and light emission by electrochemical etching. Rev Sci Instrum 75(4):837–841

52. Pienpinijtham P, Han XX, Suzuki T, Thammacharoen C, Ekgasit S, Ozaki Y (2012) Micrometer-sized gold nanoplates: starch-mediated photochemical reduction synthesis and possibility of application to tip-enhanced Raman scattering (TERS). Phys Chem Chem Phys 14(27):9636–9641

53. Kharintsev SS, Rogov AM, Kazarian SG (2013b) Nanopatterning and tuning of optical taper antenna apex for tip-enhanced Raman scattering performance. Rev Sci Instrum 84(9):093106

54. Berweger S, Atkin JM, Olmon RL, Raschke MB (2010) Adiabatic tip-Plasmon focusing for Nano-Raman spectroscopy. J Phys Chem Lett 1(24):3427–3432

55. Deckert-Gaudig T, Deckert V (2009) Ultraflat transparent gold nanoplates–ideal substrates for tip-enhanced Raman scattering experiments. Small 5(4):432–436

56. Ossikovski R, Nguyen Q, Picardi G (2007) Simple model for the polarization effects in tip-enhanced Raman spectroscopy. Phys Rev B 75(4):045412

57. Hartschuh A, Anderson N, Nobotny L (2003) Near-field Raman spectroscopy using a sharp metal tip. J Microsc 210:234–240

58. Saito Y, Hayazawa N, Kataura H, Murakami T, Tsukagoshi K, Inouye Y, Kawata S (2005) Polarization measurements in tip-enhanced Raman spectroscopy applied to single-walled carbon nanotubes. Chem Phys Lett 410(1–3):136–141

59. Yano TA, Verma P, Saito Y, Ichimura T, Kawata S (2009) Pressure-assisted tip-enhanced Raman imaging at a resolution of a few nanometres. Nat Photonics 3:473–477

60. Blum C, Schmid T, Opilik L, Weidmann S, Fagerer SR, Zenobi R (2012) Understanding tip-enhanced Raman spectra of biological molecules: a combined Raman, SERS and TERS study. J Raman Spectrosc 43(12):1895–1904

61. Sun M, Fang Y, Zhang Z, Xu H (2013) Activated vibrational modes and Fermi resonance in tip-enhanced Raman spectroscopy. Phys Rev E Stat Nonlinear Soft Matter Phys 87(2):020401

62. Sun M, Zhang Z, Chen L, Sheng S, Xu H (2014) Plasmonic gradient effects on high vacuum tip-enhanced Raman spectroscopy. Adv Opt Mater 2(1):74–80

63. Sun M, Fang Y, Yang Z, Xu H (2009) Chemical and electromagnetic mechanisms of tip-enhanced Raman scattering. Phys Chem Chem Phys 11(41):9412–9419

64. Zhang WH, Cui XD, Yeo BS, Schmid T, Hafner C, Zenobi R (2007) Nanoscale roughness on metal surfaces can increase tip-enhanced Raman scattering by an order of magnitude. Nano Lett 7(5):1401–1405

65. Ren B, Picardi G, Pettinger B, Schuster R, Ertl G (2004) Tip-enhanced Raman spectroscopy of benzenethiol adsorbed on Au and Pt single-crystal surfaces. Angew Chem Int Ed Engl 44(1):139–142

66. Love JC, Estroff LA, Kriebel JK, Nuzzo RG, Whitesides GM (2005) Self-assembled monolayers of Thiolates on metals as a form of nanotechnology. Chem Rev 105:1103–1170

67. Sun MT, Zhang SP, Fang YR, Yang ZL, Wu DY, Dong B, Xu HX (2009) Near- and deep-ultraviolet resonance Raman spectroscopy of Pyrazine-Al4 complex and Al3-Pyrazine-Al3 junction. J Phys Chem C 103:19328–19334

68. Dörfer T, Schmitt M, Popp J (2007) Deep-UV surface-enhanced Raman scattering. J Raman Spectrosc 38(11):1379–1382

69. Hecht L, Clarkson J, Smith BJE, Springett R (2006) A new single grating spectrograph for ultraviolet Raman scattering studies. J Raman Spectrosc 37(5):562–573

70. Shafaat HS, Sanchez KM, Neary TJ, Kim JE (2009) Ultraviolet resonance Raman spectroscopy of a β-sheet peptide: a model for membrane protein folding. J Raman Spectrosc 40(8):1060–1064

71. Fodor SPA, Spiro TG (1986) Ultraviolet resonance Raman spectroscopy of DNA with 200-266-nm laser excitation. J Am Chem Soc 108:3198–3205

72. Asher SA (1993) UV resonance Raman spectroscopy for analytical, physical, and biophysical chemistry. Anal Chem 65(4):201A

73. Shashilov VA, Lednev IK (2008) 2D correlation deep UV resonance Raman spectroscopy of early events of lysozyme fibrillation: kinetic mechanism and potential interpretation pitfalls. J Am Chem Soc 130:309–317

74. Huang C, Balakrishnan G, Spiro TG (2006) Protein secondary structure from deep-UV resonance Raman spectroscopy. J Raman Spectrosc 37(1–3):277–282

75. Konorov SO, Georg Schulze H, Addison CJ, Haynes CA, Blades MW, Turner RFB (2009) Ultraviolet resonance Raman spectroscopy of locked single-stranded oligo(dA) reveals conformational implications of the locked ribose in LNA. J Raman Spectrosc 40(9):1162–1171

76. Taguchi A, Hayazawa N, Furusawa K, Ishitobi H, Kawata S (2009) Deep-UV tip-enhanced Raman scattering. J Raman Spectrosc 40(9):1324–1330

77. Fujiwara A, Mizutani Y (2008) Photoinduced electron transfer in glucose oxidase: a picosecond time-resolved ultraviolet resonance Raman study. J Raman Spectrosc 39(11):1600–1605

78. Lin X, Ren B, Yang ZL, Liu GK, Tian ZQ (2005) Surface-enhanced Raman spectroscopy with ultraviolet excitation. J Raman Spectrosc 36(6–7):606–612

79. Ren B, Lin XF, Yang ZL, Liu GK, Aroca RF, Mao BW, Tian ZQ (2003) Surface-enhanced Raman scattering in the ultraviolet spectral region: UV-SERS on rhodium and ruthenium electrodes. J Am Chem Soc 125:9598–9599

80. Yang Z, Li Q, Fang Y, Sun M (2011) Deep ultraviolet tip-enhanced Raman scattering. Chem Commun (Camb) 47(32):9131–9133

81. Martin OJF, Girard C (1997) Controlling and tuning strong optical field gradients at a local probe microscope tip apex. Appl Phys Lett 70(6):705–707

82. Yang ZL, Li QH, Ren B, Tian ZQ (2011) Tunable SERS from aluminium nanohole arrays in the ultraviolet region. Chem Commun 47:3909–3911

83. Li JF, Huang YF, Ding Y, Yang ZL, Songbo L, Zhou XS, Fan FR, Zhang W, Zhou ZY, Wu DY, Ren B, Wang ZL, Zhong QT (2010) Shell-isolated nanoparticle-enhanced Raman spectroscopy. Nature 464:392–395

84. Kim K, Lee I, Lee SJ (2003) Photolytic reduction of 4-nitrobenzenethiol on Au mediated via Ag nanoparticles. Chem Phys Lett 377(1–2):201–204

85. Steidtner J, Pettinger B (2007) High-resolution microscope for tip-enhanced optical processes in ultrahigh vacuum. Rev Sci Instrum 78(10):103104

86. Jiang N, Foley ET, Klingsporn JM, Sonntag MD, Valley NA, Dieringer JA, Seideman T, Schatz GC, Hersam MC, Van Duyne RP (2012) Correction to observation of multiple vibrational modes in ultrahigh vacuum tip-enhanced Raman spectroscopy combined with molecular-resolution scanning tunneling microscopy. Nano Lett 12(12):6506–6506

87. Lin XD, Uzayisenga V, Li JF, Fang P-P, Wu DY, Ren B, Tian ZQ (2012) Synthesis of ultrathin and compact Au@MnO2 nanoparticles for shell-isolated nanoparticle-enhanced Raman spectroscopy (SHINERS). J Raman Spectrosc 43(1):40–45

88. Knight MW, Sobhani H, Nordlander P, Halas NJ (2011) Photodetection with active optical antennas. Science 332:702–704

89. Zhang Z, Xu P, Yang X, Liang W, Sun M (2016) Surface plasmon-driven photocatalysis in ambient, aqueous and high-vacuum monitored by SERS and TERS. J Photochem Photobiol C: Photochem Rev 27:100–112

90. Sun M, Xu H (2012) A novel application of plasmonics: plasmon-driven surface-catalyzed reactions. Small 8(18):2777–2786

91. Zhang Z, Deckert-Gaudig T, Singh P, Deckert V (2015) Single molecule level plasmonic catalysis - a dilution study of p-nitrothiophenol on gold dimers. Chem Commun (Camb) 51(15):3069–3072

92. Fang Y, Li Y, Xu H, Sun M (2010) Ascertaining p,p'-dimercaptoazobenzene produced from p-aminothiophenol by selective catalytic coupling reaction on silver nanoparticles. Langmuir 26(11):7737–7746

93. Huang YF, Zhu HP, Liu GK, Wu DY, Ren B, Tian ZQ (2010) When the signal is not from the original molecule to be detected: chemical transformation of para-Aminothiophenol on Ag during the SERS measurement. J Am Chem Soc 132:9244–9246

94. Dai Z, Xiao XH, Wu W, Zhang YP, Liao L, Guo SS, Ying JJ, Shan CX, Sun MT, Jiang CZ (2015) Plasmon-driven reaction controlled by the number of graphene layers and localized surface plasmon distribution during optical excitation. Light: Sci Appl 4(10):e342

95. Kang L, Chu J, Zhao H, Xu P, Sun M (2015) Recent progress in the applications of graphene in surface-enhanced Raman scattering and plasmon-induced catalytic reactions. J Mater Chem C 3(35):9024–9037

96. Ding Q, Shi Y, Chen M, Li H, Yang X, Qu Y, Liang W, Sun M (2016) Ultrafast dynamics of Plasmon-Exciton interaction of Ag nanowire- Graphene hybrids for surface catalytic reactions. Sci Rep 6:32724

97. Sun M, Zhang Z, Wang P, Li Q, Ma F, Xu H (2013) Remotely excited Raman optical activity using chiral plasmon propagation in Ag nanowires. Light: Sci Appl 2(11):e112

98. Huang Y, Fang Y, Zhang Z, Zhu L, Sun M (2014) Nanowire-supported plasmonic waveguide for remote excitation of surface-enhanced Raman scattering. Light: Sci Appl 3(8):e199

99. Zhang Z, Fang Y, Wang W, Chen L, Sun M (2016) Propagating surface Plasmon Polaritons: towards applications for remote-excitation surface catalytic reactions. Adv Sci (Weinh) 3(1):1500215

100. Ichimura T, Hayazawa N, Hashimoto M, Inouye Y, Kawata S (2004) Tip-enhanced coherent anti-stokes Raman scattering for vibrational nanoimaging. Phys Rev Lett 92(22):220801

101. Dong B, Fang Y, Xia L, Xu H, Sun M (2011) Is 4-nitrobenzenethiol converted to p,p′-dimercaptoazobenzene or 4-aminothiophenol by surface photochemistry reaction? J Raman Spectrosc 42(6):1205–1206

102. Merlen A, Chaigneau M, Coussan S (2015) Vibrational modes of aminothiophenol: a TERS and DFT study. Phys Chem Chem Phys 17(29):19134–19138

103. Zhang Z, Sun M, Ruan P, Zheng H, Xu H (2013c) Electric field gradient quadrupole Raman modes observed in plasmon-driven catalytic reactions revealed by HV-TERS. Nanoscale 5(10):4151–4155

104. Kumar N, Stephanidis B, Zenobi R, Wain AJ, Roy D (2015) Nanoscale mapping of catalytic activity using tip-enhanced Raman spectroscopy. Nano 7(16):7133–7137

105. Fujimori H, Kakihana M, Ioku K, Goto S, Yoshimura M (2001) Advantage of anti-stokes Raman scattering for high-temperature measurements. Appl Phys Lett 79(7):937–939

106. Moskovits M, DiLella DP (1980) Surface-enhanced Raman spectroscopy of benzene and benzene-d6 adsorbed on silver. J Chem Phys 73(12):6068–6075

107. Moskovits M, DiLella DP (1982) Intense quadrupole transitions in the spectra of molecules near metal surfaces. J Chem Phys 77(4): 1655–1660

108. Christopher P, Xin H, Linic S (2011) Nat Chem 3:467

109. Ayars E, Hallen HD (2000) Electric field gradient effects in Raman spectroscopy. Phys Rev Lett 85(19):4180–4183

110. Kim H, Kosuda KM, Van Duyne RP, Stair PC (2010) Resonance Raman and surface- and tip-enhanced Raman spectroscopy methods to study solid catalysts and heterogeneous catalytic reactions. Chem Soc Rev 39(12):4820–4844

111. Pallaoro A, Braun GB, Reich NO, Moskovits M (2010) Mapping local pH in live cells using encapsulated fluorescent SERS nanotags. Small 6:618

112. Sun M, Huang Y, Xia L, Chen X, Xu H (2011) The pH-controlled plasmon-assisted surface photocatalysis reaction of 4-aminothiophenol top, p′-dimercaptoazobenzene on Au, Ag, and Cu Colloids. J Phys Chem C 115(19):9629–9636

113. Gao S, Ueno K, Misawa H (2011) Plasmonic antenna effects on photochemical reactions. Acc Chem Res 44:251

114. Buckingham AD (1967) Adv Chem Phys 12:107

115. Fleischmann M, Hendra PJ, Quillan M (1974) Raman spectra of pyridine adsorbed at a silver electrode. Chem Phys Lett 26:163–166

116. Jeanmaire DL, Van Duyne RP (1977) Surface Raman spectroelectrochemistry. J Electroanal Chem Interfacial Electrochem 84(1):1–20

117. Campion A, Kambhampati P (1998) Surface-enhanced Raman scattering. Chem Soc Rev 27:241–250

118. Campion A, Kambhampati P (1985) Surface-enhanced Raman scattering. J Opt Soc Am B 2:1538–1541